ACS APPLIED MATERIALS & INTERFACES

Research Article

www.acsami.org

Aqueous Solution-Processed GeO_2: An Anode Interfacial Layer for High Performance and Air-Stable Organic Solar Cells

Mei-Feng Xu, Xiao-Bo Shi, Zhi-Ming Jin, Feng-Shuo Zu, Yang Liu, Lei Zhang, Zhao-Kui Wang,* and Liang-Sheng Liao*

Jiangsu Key Laboratory for Carbon-Based Functional Materials & Devices, Institute of Functional Nano & Soft Materials (FUNSOM), Soochow University, Suzhou, Jiangsu, 215123 China

Supporting Information

ABSTRACT: A simple and cheap method for depositing solution-processed GeO_2 ($sGeO_2$) film is proposed utilizing the weak solubility of GeO_2 in water. X-ray photoelectron spectroscopy analysis reveals that a pure GeO_2 thin film can be formed by casting its aqueous solution. This method can avoid the difficulty of vacuum evaporation by its high melting point. The $sGeO_2$ film has been used successfully as an anode interfacial layer in poly(3-hexylthiophene) (P3HT) and indene-C_{60} bisadduct ($IC_{60}BA$)-based bulk heterojunction organic solar cells with improved power conversion efficiency and device stability compared with that using conventional poly (3,4-ethylenedioxythiophene):poly (styrenesulfonate) (PEDOT:PSS); the improvement of the power conversion efficiency and the device stability are estimated to be 9% and 50%, respectively. The calculations of optical intensity in a whole cell demonstrate that a thin layer of $sGeO_2$ could function as an optical spacer in the based bulk heterojunction (BHJ) organic solar cells (OSCs) for enhancing the light harvesting in the active layer. Interfacial evaluation by impedance spectroscopy shows that the $sGeO_2$-based cell exists less charge carrier recombination and lower contact resistance. More importantly, the $sGeO_2$ film processing is very simple and environmentally friendly, which has potential applications in green and low-cost organic electronics in the future.

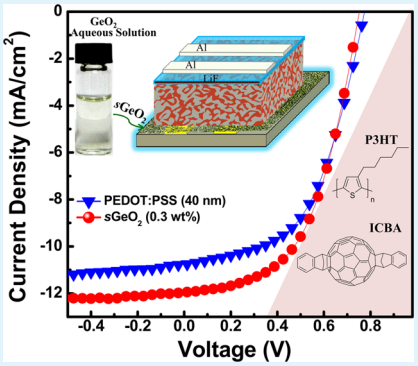

KEYWORDS: *organic solar cells, interfacial layer, solution processing, GeO_2 aqueous solution, device stability, optical space effect*

1. INTRODUCTION

Transition metal oxides (TMOs)-based inorganic materials, such as molybdenum oxide (MoO_3), vanadium oxide (V_2O_5), tungsten oxide (WO_3), and nickel oxide (NiO), have been widely used in organic electronics[1−11] since the initial report of significant increases in hole-injection when using thin film of MoO_3 as an anode interlayer in organic light emitting diodes (OLEDs) by Tokito et al.[12] Recently, it is also reported that these TMO materials are the potential alternatives to replace the conventional poly (3,4-ethylenedioxythiophene):poly (styrenesulfonate) (PEDOT:PSS) in organic electronics with the goal of improving device stability for avoiding the acidic nature of the aqueous PEDOT:PSS dispersions.[13−16]

As a good semiconductor material, germanium dioxide (GeO_2) also has potential applications in organic electronics like the aforementioned TMOs owing to its good hole mobility and transparency in visible light range. For its suitable energy level,[17,18] GeO_2 is expected to act as a hole extracting layer and electron blocking layer simultaneously in organic electronics. Unfortunately, the tentative application of GeO_2 as an interfacial layer demonstrated unsatisfactory effects in OLEDs[19] and organic solar cells (OSCs)[20] due to its poor film-processing ability previously. When thermally evaporating GeO_2 with a vacuum process, the chamber pressure is too high for reliable device fabrication because of its high melting temperature (1115 °C) and boiling temperature (1200 °C). Actually, a thin GeO_2 film is usually deposited by magnetron sputtering or pulsed laser deposition techniques, which are unsuitable for organic electronics from the viewpoints of device processing.

Recently, solution-processed TMO materials (i.e., MoO_3) attract much attention in OSCs because comparable efficiency and improved device stability can be achieved compared to PEDOT:PSS-based cells.[21−26] However, these solution-processed TMOs are generally prepared by a hydration method using different metal oxide precursors[21−23] and/or sol-gel-based colloidal suspensions with the aid of organic solvents.[24−26] The preparation processes are still complicated with higher annealing temperature. In addition, the necessary organic solvents are unfriendly to the environments.

Herein, we demonstrate a very simple means for preparing the GeO_2 aqueous solution by utilizing the weak solubility of GeO_2 in water.[27−31] A uniform and transparent GeO_2 aqueous solution can be obtained easily just dissolving the commercial GeO_2 powder into the deionized water, which makes it possible to easily deposit the GeO_2 film through the solution-processed method and avoids the difficulty of vacuum evaporation by its high melting temperature. In addition, the water, as a kind of

Received: July 26, 2013
Accepted: October 9, 2013
Published: October 9, 2013

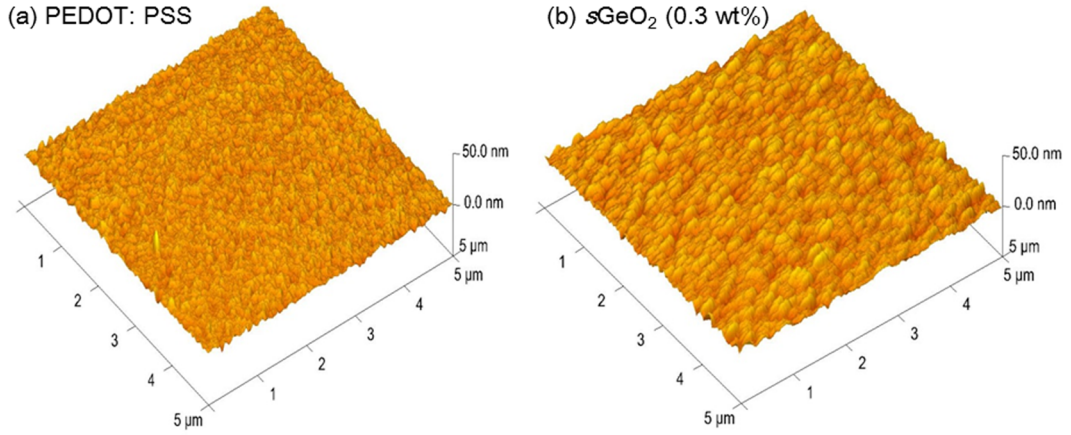

Figure 1. AFM height images of PEDOT:PSS (40 nm) and sGeO$_2$ film casting from 0.30 wt % GeO$_2$ aqueous solution.

cheap and green solvent, is easily accessible and environmentally friendly. The aqueous solution-processed GeO$_2$ (sGeO$_2$) films are successfully used as an anode interfacial layer in poly(3-hexylthiophene) (P3HT) and indene-C$_{60}$ bisadduct (IC$_{60}$BA)-based bulk heterojunction (BHJ) OSCs. In particular, the devices containing a sGeO$_2$ interfacial layer exhibit improved power conversion efficiency and device stability in comparison with the device using the conventional PEDOT:PSS.

2. EXPERIMENTAL SECTION

2.1. OSC Fabrication. Devices with structures of ITO/sGeO$_2$ (or PEDOT:PSS 40 nm)/P3HT: IC$_{60}$BA (110 nm)/LiF (0.5 nm)/Al (100 nm) were fabricated to investigate the functions of sGeO$_2$. Hole-dominated devices with structures of ITO/sGeO$_2$ (or PEDOT:PSS 40 nm)/P3HT:IC$_{60}$BA (110 nm)/MoO$_3$ (20 nm)/Al (100 nm) were fabricated to investigate the interfacial properties through the measurements of impedance spectroscopy and the current density–voltage (J–V) characteristics with varied temperature. The patterned ITO was cleaned by acetone, ethanol, and deionized water sequentially. After oven drying, the ITO surface was treated with ultraviolet ozone for 10 min. GeO$_2$ and PEDOT:PSS solution were then spin-coated onto the ITO at 4000 rpm for 60 s and annealed at 120 °C for 10 min in air. The active layer was spin-coated at 700 rpm for 50 s from a solution of P3HT: IC$_{60}$BA (19 mg/mL, 1:1 by volume) in dichlorobenzene in a glove box. The LiF and Al were deposited, respectively, in a deposition chamber under a base vacuum pressure lower than 2×10^{-6} Torr.

2.2. Measurements. AFM images using a Veeco Multimode V instrument were obtained to evaluate the surface morphology of sGeO$_2$ and PEDOT:PSS films. XPS analysis was obtained using a Kratos AXIS UltraDLD ultrahigh vacuum (UHV) surface analysis system with a monochromatic aluminum Kα source (1486.6 eV). UPS analysis was carried out with an unfiltered He I (21.2 eV) gas discharge lamp and a hemispherical analyzer. The transmittance spectra of sGeO$_2$ and PEDOT:PSS films were measured with an UV/Vis spectrophotometer (PerkinElmer Lambda 750). J–V characteristics of OSC devices under 1 Sun illumination were performed in the N$_2$ glove box using a programmable Keithley 2400 source meter under AM 1.5G solar irradiation at 100 mW cm^{-2} (Newport, Class AAA solar simulator, 94023A-U). The stabilities of OSCs devices without encapsulation were evaluated under continuous irradiation by an incandescent lamp (in intensity of 52 mW cm^{-2}) in air under ambient conditions. The optical field ($|E|^2$) calculations in whole BHJ OSC devices were carried out by a classic transfer matrix method. Impedance spectroscopy (IS) measurements were performed using a Wayne Kerr 6550B precision impedance analyzer with a 50 mV perturbation oscillation signal in a frequency range from 50 Hz to 20 MHz.

3. RESULTS AND DISCUSSION

3.1. Aqueous Solution-Processed GeO$_2$ Film. In general, the TMO interfacial layer in OSCs with optimized performance is very thin with nanometer scale.[1−12,21−26] Although it has a weak solubility of GeO$_2$ in water (i.e., 0.43 g in 100 g of H$_2$O at 20 °C),[32] it provides an opportunity for GeO$_2$ to deposit as a thin film via solution processing. In this report, we demonstrate an aqueous solution-processed GeO$_2$ (sGeO$_2$) film as an anode interfacial layer in poly(3-hexylthiophene) (P3HT) and indene-C$_{60}$ bisadduct (IC$_{60}$BA)-based bulk heterojunction (BHJ) OSCs. A uniform and transparent GeO$_2$ aqueous solution can be obtained easily by just dissolving the commercial GeO$_2$ powder into the deionized water. The water, as a green solvent, is easily accessible and environmentally friendly. In particular, we show that devices containing a sGeO$_2$ interfacial layer exhibit improved power conversion efficiency and device stability in comparison with the device using the conventional PEDOT:PSS. Clevios P VP Al 4083 PEDOT:PSS was bought from Heraeus (Germany). P3HT and ICBA were both obtained from Luminescence Technology Crop. (Taiwan); PC$_{61}$BM was produced by Nichem Fine Technology Co. Ltd. (Taiwan), and 1,2-dichlorobenzene (product of J&K Chemical, China) was used to dissolve the polymers and the derivatives of fullerenes. GeO$_2$ power was provide by Shanghai Chemical Industry Co. (China). GeO$_2$ aqueous solutions (0.10−0.50 wt %) were prepared by directly dissolving GeO$_2$ powder into deionized water in air. The thickness of the GeO$_2$ films is between 3 and 8 nm for different concentrations. A weak hydrolysis reaction occurred as follows:[33]

$$GeO_2 + 2H_2O = Ge(OH)_4 \quad (1)$$

The solution pH value is about 7 owing to the formation of almost neutral germanium hydroxide species in GeO$_2$ aqueous solution.[33] The neutral solution suggests possible improvements in OSCs' stabilities if using sGeO$_2$ as an interfacial layer. sGeO$_2$ films were formed by casting the GeO$_2$ aqueous solutions onto ITO glass and treated at 120 °C for 10 minutes subsequently. The deposited sGeO$_2$ film was very transparent (>96%) in the whole visible spectral region (Figure S1, Supporting Information) for sufficient light passing into the active layer through ITO/sGeO$_2$ layers.

Figure 1 shows the atomic force microscopy (AFM) surface morphologies of PEDOT:PSS (40 nm) and sGeO$_2$ films deposited from 0.30 wt % GeO$_2$ aqueous solutions. The surface

roughness (in Root-Mean-Square, RMS) of PEDOT:PSS and sGeO$_2$ is 2.13 and 2.19 nm, respectively, which are both smaller than that of ITO (4.35 nm). In addition, no large difference of surface roughness appears with varied GeO$_2$ solution concentrations (Figure S2, Supporting Information). It means that the aqueous solution processing can provide a smooth sGeO$_2$ film, which is beneficial for device performance and stability.

X-ray photoelectron spectroscopy (XPS) and ultraviolet photoelectron spectroscopy (UPS) measurements were carried out to confirm the main component in sGeO$_2$ film. The full scanning XPS spectra for ITO substrate and the sGeO$_2$ film made from 0.30 wt % GeO$_2$ aqueous solution are shown in Figure 2a. All peak positions were calibrated by referencing to

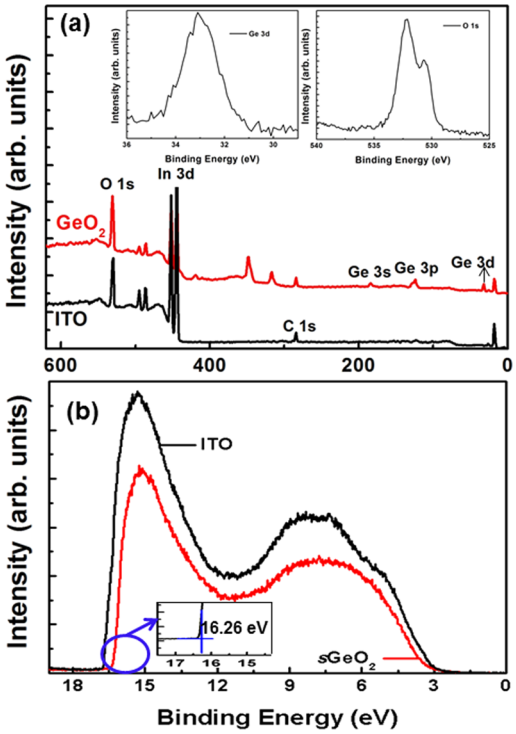

Figure 2. Full scanning XPS and UPS spectra for ITO substrate and the sGeO$_2$ film made from 0.30 wt % GeO$_2$ aqueous solution. The inset of (a) shows the narrow spectra of Ge 3d and O 1s in the sGeO$_2$ film, and the inset of (b) magnifies the secondary-electron cutoffs.

C 1s core level located at 284.5 eV. The insets show the narrow spectra of Ge 3d and O 1s in the sGeO$_2$ film. The core level locates at 33.1 eV, which is in perfect agreement with those reported in the literature for pure GeO$_2$.[34,35] No other germanium suboxides were detected in sGeO$_2$ film indicating a pure germanium dioxide film could be obtained by direct casting of GeO$_2$ aqueous solution. The UPS measurement of ITO substrate and sGeO$_2$ film were carried out, and the results are shown in Figure 2b, where the inset is the magnified region of the photoemission cut-off. The work function of sGeO$_2$ film (air-exposed) was found to be 4.94 eV from the photoemission cut-off, which is lower than the in situ value due to its sensitivity to oxygen, moisture, and so on.[8] The work function of ITO substrate was measured as 4.5 eV, which is also lower than its usual value.

3.2. Photovoltaic Performance. P3HT:IC$_{60}$BA-based BHJ OSCs containing sGeO$_2$ layers were fabricated for evaluating the interfacial function of sGeO$_2$ on ITO. Reference devices with the conventional PEDOT:PSS (40 nm) and without any interfacial layer were also fabricated for comparison. The J–V characteristics of all devices under AM 1.5G illumination with light intensity of 100 mW cm^{-2} are shown in Figure 3a. The key cell paremeters in these devices

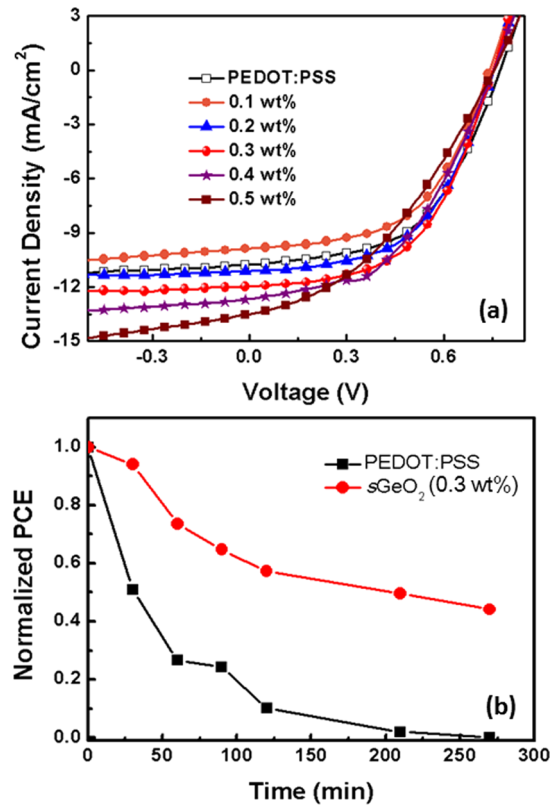

Figure 3. (a) J–V characteristics in P3HT:IC$_{60}$BA-based BHJ OSCs with 40 nm PEDOT:PSS and with sGeO$_2$ layers (fabrication from GeO$_2$ aqueous solution with different concentrations) under AM 1.5G illumination with light intensity of 100 mW cm^{-2}. (b) The normalized PCE vaules as a function of illuminating time in the devices using 40 nm PEDOT:PSS and sGeO$_2$ (fabrication from 0.30 wt % GeO$_2$ aqueous solution), respectively.

are listed in Table 1. The reference device using PEDOT:PSS as an ITO modification layer showed a power conversion efficiency (PCE) of 4.41% with an open circuit voltage (V_{oc}) of

Table 1. Comparison of Device Performance[a]

interlayer	thickness (nm)	V_{oc} (V)	J_{sc} (mA/cm^2)	FF (%)	PCE (%)
PEDOT:PSS	40	0.76	10.75	54	4.41
0.1 wt %	3	0.74	9.86	54	3.94
0.2 wt %	4	0.75	11.11	54	4.51
0.3 wt %	5	0.75	11.94	54	4.80
0.4 wt %	6	0.75	12.63	45	4.20
0.5 wt %	8	0.75	13.46	39	3.95

[a]This table shows the open-circuit voltage (V_{oc}), short-circuit current density (J_{sc}), fill factor (FF), and power conversion efficiency (PCE) of the reference device (the device using 40 nm PEDOT:PSS) and the device using sGeO$_2$ (fabricated from GeO$_2$ aqueous solution with different concentrations) under AM 1.5G illumination with light intensity of 100 mW cm^{-2}.

0.76 V, a short circuit current density (J_{sc}) of 10.75 mA cm^{-2}, and a fill factor (FF) of 54%, respectively. In the cases of using sGeO$_2$ as the interlayer, J_{sc} was increased from 9.86 to 13.46 mA cm^{-2} with the concentration of 0.5 wt % GeO$_2$ aqueous solution. Meanwhile, V_{oc} (~0.75 V) is comparable with that in a PEDOT:PSS-based cell. Noticeably, FF in sGeO$_2$-based cells began to deteriorate from the concontration of 0.30 wt %. However, there was no large change in V_{oc}, while there was an enhanced trend in J_{sc} when increasing the GeO$_2$ concentration. Therefore, we ascribed the worse cell efficiency in the case of high concentrations of GeO$_2$ aqueous solutions to be the poor surface morphology and interface contact between the sGeO$_2$ and the active layer due to incomplete solubility of GeO$_2$ in water. In all, the sGeO$_2$-based cell showed a PCE of 4.80%, which was higher than that of the reference device (4.41%), at an optimized concentration of 0.30 wt %. (The PCE is 3.31% for the reference device without any interfacial layer as shown in Figure S6, Supporting Information.)

As mentioned above, improved device stability is expected in the devices containing sGeO$_2$ thin layers. The normalized PCE as a function of operational time in PEDOT:PSS- and 0.30 wt % sGeO$_2$-based OSCs were shown in Figure 3b. The measurements were carried out under continuous white-light soaking with an intensity of 52 mW cm^{-2} in air without encapsulation. The cell using PEDOT:PSS decayed rapidly in the initial 120 minutes, resulting in almost 90% decrease in PCE, where as just a 40% decrease in PCE was observed in the sGeO$_2$-based cell. After continuous light-soaking with 270 min, the device containing sGeO$_2$ still had a half value of initial PCE. In contrast, nearly no PCE was observed in the PEDOT:PSS-based device. The decay conditions for other cell parameters including J_{sc}, V_{oc}, and FF can be seen in Figure S3, Supporting Information. The experimental results demonstrated that a thin sGeO$_2$ film can act as an efficient interlayer in BHJ OSCs with the goal of high and stable device performance.

The stability improvement in the sGeO$_2$-based cell is easily understood and attributed to almost neutral GeO$_2$ aqueous solution compared to the acidic hygroscopic nature of the aqueous PEDOT:PSS dispersion.[13−16,33] The device performances indicate that the improved PCE in the devices using sGeO$_2$ compared to PEDOT:PSS is originated from a modest increase in J_{sc}. We mainly ascribe the improved J_{sc} to following several factors. One is the better electron-blocking ability of GeO$_2$ than that of PEDOT:PSS owing to the large band gap (GeO$_2$: 5.20−5.95 eV).[36] The other ones are the optical spacer effect of the thin sGeO$_2$ and the good interface contact at ITO/sGeO$_2$. To confirm them, the evaluations of optical intensity distribution in the whole cell and the anode interface conditions were carried out as follows.

3.3. Calculations of Optical Intensity Distribution. It is known that the optical interference effect plays an important role on the optical intensity distribution in thin film devices when the layer thicknesses are comparable to the absorption depth and/or the incident light wavelength.[37−43] The optical intensity distribution in the devices affects the generation conditions of electron-hole pairs near the interface of ITO/PEDOT:PSS, which will deteriorate the device efficiency.[44−47] Insertion of an optical spacer has been proven to be an efficient approach to change the device architecture with the goal of desired light intensity redistribution inside the device.[42−53] We assume that the increased J_{sc} in the present case was associated with the optical spacer effect from the thin sGeO$_2$ layer.

To validate the assumption, the classic transfer matrix method (TMM)[40−43] was used to calculate the optical field ($|E|^2$) distribution in whole cell. A typical optical field plot for a single light wavelength of 550 nm in sGeO$_2$- and PEDOT:PSS-based devices were shown in Figure 4. The optical constants (n:

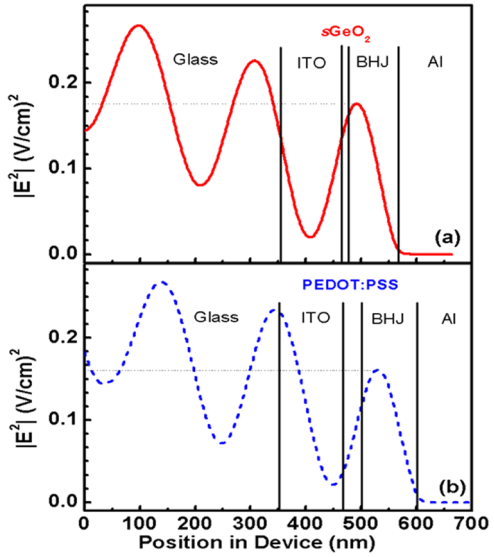

Figure 4. Optical field ($|E|^2$) distributions calculated by the transfer matrix method (TMM) in P3HT:IC$_{60}$BA-based BHJ devices (a) using sGeO$_2$ with a concentration of 0.30% and (b) using PEDOT:PSS as anode interfacial layers (under the consideration of a 550 nm incoming light wave incidenced from the left).

refractive index; k: extinction coefficient) of P3HT:IC$_{60}$BA BHJ active layer, sGeO$_2$, and PEDOT:PSS, which were necessary for the optical field calculation, measured by spectroscopic ellipsometry were shown in Figure 5. Compared to the

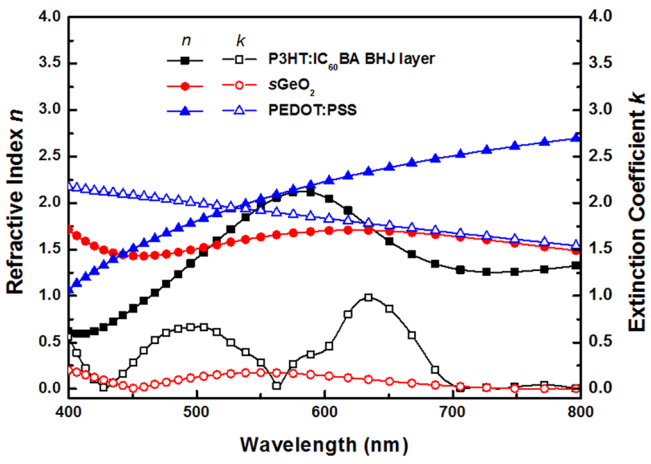

Figure 5. Optical constants (n: refractive index; k: extinction coefficient) of P3HT:IC$_{60}$BA BHJ active layer, 0.30 wt % sGeO$_2$, and PEDOT:PSS measured by spectroscopic ellipsometry.

PEDOT:PSS (40 nm)-based device, an enhanced optical field in the active layer was observed in the device using thin sGeO$_2$ (5 nm), which can enhance photon harvesting and result in improved J_{sc}. As mentioned above, the transmittance of the thin sGeO$_2$ is slightly larger than that of 40 nm PEDOT:PSS. In addition, from Figure 5, the extinction coefficient of sGeO$_2$ is also smaller than that of PEDOT:PSS in the whole visible

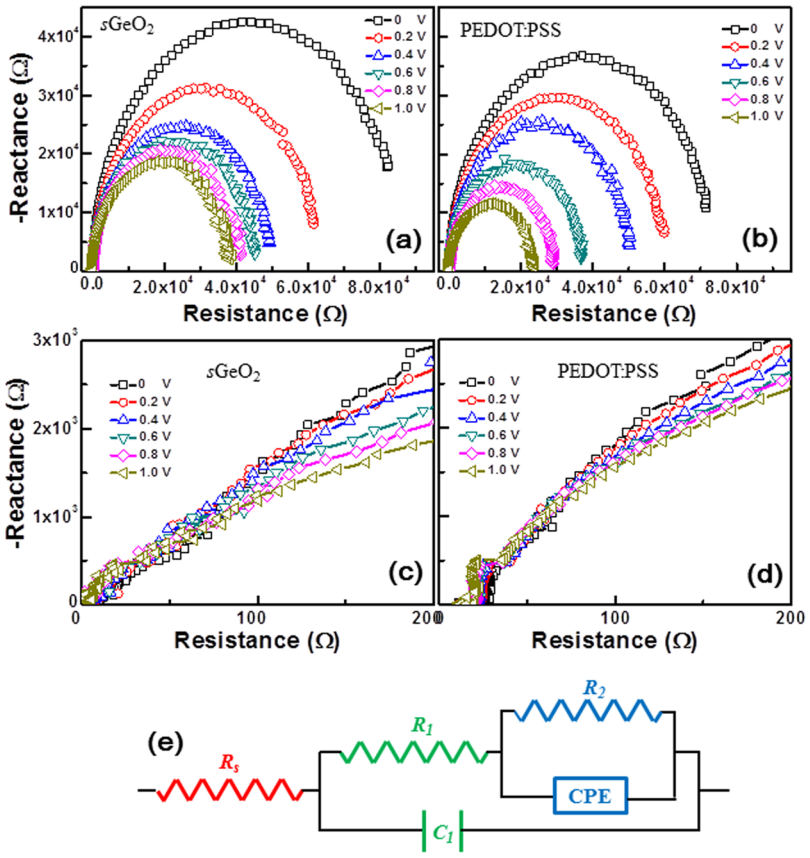

Figure 6. Impedance response in P3HT:$IC_{60}BA$-based hole-dominant devices (a) using 0.30 wt % $s$$GeO_2$ and (b) using PEDOT:PSS as anode interfacial layers at varied sample bias under dark condition. (e) Equivalent circuit used to fit the data in (a) and (b). (c,d) High frequency portion of (a) and (b), respectively. R_s represents the resistive losses in the ITO and $s$$GeO_2$ (or PEDOT:PSS); $R_1||C_1$ combination (corresponding to high frequency arc) is related to the bulk resistance and a capacitance that includes both a geometric component and a second component related to photoexcitation events in the film. $R_2||$CPE combination corresponds the low frequency arc which relates to a recombination resistance and chemical capacitance that are associated with the internal charge transfer events at the donor/acceptor interfaces.

spectral range. Therefore, the total absorption in the interfacial layer is suppressed, resulting in an enhanced optical field within the BHJ layer in the $s$$GeO_2$-based device. The general case for optical field distribution considering all the wavelengths (300−900 nm) exhibited a similar behavior (Figure S4, Supporting Information).

3.4. Anode Interface Evaluations. Further evaluations by impedance spectroscopy (IS), which is a powerful technique for investigating the electric and interfacial properties in thin film devices,[54−69] were carried out to clarify how the $s$$GeO_2$ thin layer functions as an effective interfacial layer in OSCs. Two hole-dominant devices with structure of ITO/$s$$GeO_2$(or PEDOT:PSS)/P3HT:$IC_{60}BA$/$MoO_3$/Al were fabricated to investigate the anode interface behavior, $s$$GeO_2$ with a concentration of 0.30 wt %. The Cole−Cole plots of the impedence responses in two devices were shown in Figure 6. The IS data were modeled by an equivalent circuit shown in Figure 6e, corresponding to the large arc in Figure 6a,b and small arc in Figure 6c,d. The representations of circuit elements in the equivalent circuit can be seen elsewhere.[54−57] The model of a constant phase element (CPE) in parallel with a recombination resistor (R_2), which is closer to the physical process in actual devices, is usually used to describe the charge transfer conditions in the active layer.[58−63] From Figure 6c,d, the series resistor (R_S) at zero bias in $s$$GeO_2$- and PEDOT:PSS-based cell was determined to be 11 and 28.2 Ω, respectively. The detailed values of all circuit elements in two devices can be seen in Table 2. There existed a smaller interface resistance in $s$$GeO_2$-based devices. It suggests that there is a good interface contact in the device using $s$$GeO_2$ compared to the PEDOT:PSS-based one.

Table 2. Extrapolated Values of All Circuit Elements Including Series Resistor (R_S), Bulk Resistance (R_1), Recombination Resistance (R_2), and Constant Phase Element (CPE) under Bias 0 V in the Equivalent Circuits

circuit element	PEDOT:PSS-based device	$s$$GeO_2$-based device
R_s (Ω)	28.2	11.0
R_1 (Ω)	76.8	80.6
R_2 (kΩ)	128	337
CPE	3.4×10^{-9}	4.1×10^{-9}

Furthermore, the $J-V$ characteristics in the temperature range of 153−273 K in $s$$GeO_2$- and PEDOT:PSS-based hole-dominated devices were measured and shown in Figure 7a,b, respectively. The temperature-dependent $J-V$ curves generally associate with a Schottky thermal emission current in the device. The charge injection behavior is commonly strongly affected by complicated interface conditions caused by chemical, structural, and morphological factors. Although the Schottky thermionic emission model is not a realistic theory, it provides a trend of barrier change with different modification on ITO. Therefore, we extrapolate the barrier heights at

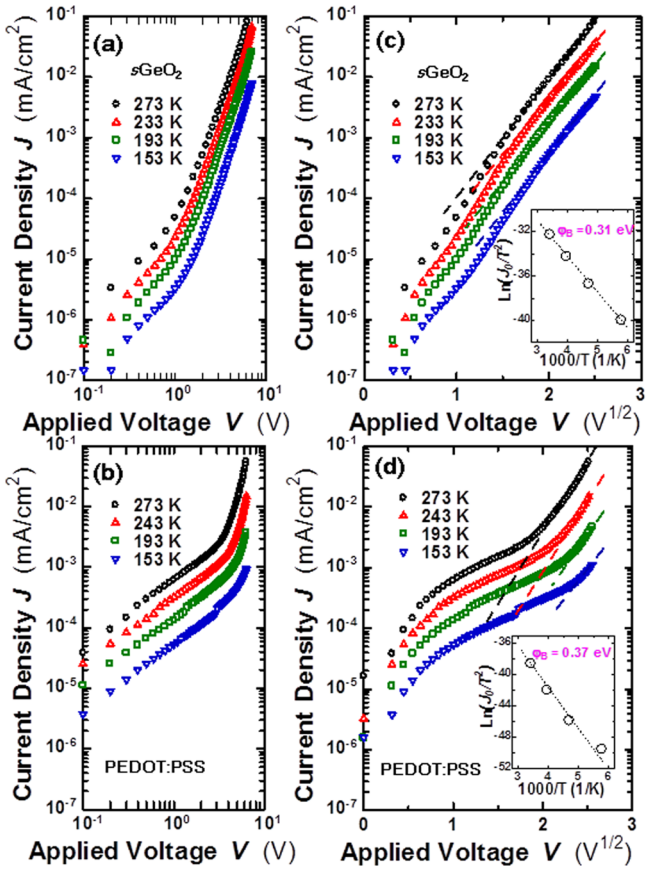

Figure 7. Temperature dependence of $J-V$ characteristics in P3HT:$IC_{60}BA$-based hole-dominant devices (a) using $s$$GeO_2$ (0.30 wt %) and (b) using PEDOT:PSS (40 nm) as anode interfacial layers. (c,d) The relationship between ln$J$ and $V^{1/2}$ for the data in (a) and (b), respectively. Insets of (c) and (d) are the corresponding relationships between $\ln J_0/T^2$ and $1/T$, respectively. J_0 was obtained by extrapolating in $V = 0$ from (c) and (d).

interfaces of ITO/$s$$GeO_2$ (or PEDOT:PSS) by a Schottky thermal emission model[69] in high bias region through the temperature-dependent $J-V$ data in Figure 7a,b. The details can be seen elsewhere.[70−72] Figure 7c,d show the relationship of ln$J$ vs $V^{1/2}$ corresponding to the data in Figure 7a,b. Insets are the relationships of $\ln J_0/T^2$ vs $1/T$, where T is the temperature and J_0 is the current densities at zero voltage under different temperature by extrapolating straight lines to the ordinal point in Figure 7a,b. The slope of the extrapolated line in the insets give the barrier height of 0.31 and 0.37 eV in $s$$GeO_2$- and PEDOT:PSS-based hole-dominated devices, respectively, which is consist with the results of interface resistances evaluation.

In addition, the recombination resistance R_2 is generally related to whether the generated charge carriers will be extracted to the electrodes or be recombinated in the active layer.[37,57] When R_2 is smaller than the bulk resistance R_1, charge carriers generated in the active layer are more likely to be recombined than to be collected.[57] In present work, R_1 in two devices was similar (about 80 Ω), while R_2 in the $s$$GeO_2$-based device is 2 times larger than that in the PEDOT:PSS-based device. It demonstrated that the carrier recombination in the PEDOT:PSS-based device was more serious than that in the $s$$GeO_2$-based device, which was supported by the results of carrier lifetime evaluations from the reactance−frequency relation in two devices as shown in Figure 8. In a word, an improved anode interface contact can be formed and the carrier recombination can be suppressed to some extent in the cell using $s$$GeO_2$ compared to PEDOT:PSS.

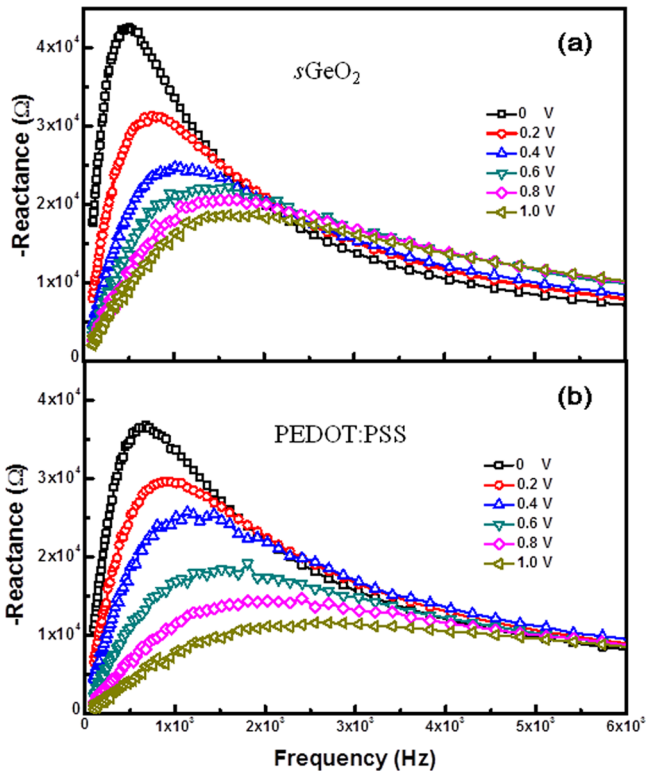

Figure 8. Reactance−frequency relation in P3HT:$IC_{60}BA$-based hole-dominant devices (a) using $s$$GeO_2$ (0.30 wt %) and (b) using PEDOT:PSS (40 nm) as anode interfacial layers at varied sample bias under dark condition. The average charge carrier lifetime is related to the frequency at which the reactance reaches its peak value.

Therefore, the imporved device performance by using a soluton-processed GeO_2 interfacial layer is mainly attributed to the better electron-blocking of $s$$GeO_2$, the optical spacer effect of $s$$GeO_2$, and the good interface contact at ITO/$s$$GeO_2$. From Figure 3 and Table 1, V_{oc} is unchangeable and J_{sc} is increased with an increase in the GeO_2 concentration, while FF is deteriorated when the GeO_2 concentration is larger than 0.3 wt %. In these devices, electron-blocking ability of GeO_2 and enhanced optical field (the increased J_{sc} with increasing GeO_2 concentration mainly depends on optical field distribution) still exist, but the device performance decreased, which is due to the relatively large resistance. Therefore, the interface factor plays the most important role in the performance improvement, while the electron-blocking effect of $s$$GeO_2$ and the optical spacer effect of $s$$GeO_2$ also have some effect on the device performance.

4. CONCLUSION

In summary, we have demonstrated a very simple route to deposit GeO_2 thin film from its aqueous solution. The XPS data demonstrated that a pure GeO_2 film could be achieved by casting its aqueous solution. The UPS measurement demonstrates that a $s$$GeO_2$ layer act as a hole-extracting layer and an electron-blocking layer simultaneously for its suitable energy level. $s$$GeO_2$ is successfully used as an anode interlayer in

P3HT: $IC_{60}BA$-based BHJ OSCs with enhanced power convension efficiency and improved device stability compared to the conventional PEDOT:PSS; the improvement of the power conversion efficiency and the device stability are estimated to be 9% and 50%, respectively. The optical intensity calculation through the transfer matrix method reveals that a thin $sGeO_2$ can function as an optical spacer in BHJ OSCs for enhancing the light harvesting in the active layer. Interfacial evaluations by impedance spectroscopy also show that a superior interface contact could be formed in devices using $sGeO_2$ compared to PEDOT:PSS. In particular, the preparation of GeO_2 aqueous solution is very simple just directly dissolving the commercial GeO_2 powder into deionized water. The deposition of a thin GeO_2 can be realized easily by its aqueous solution without any vacuum processing by avoiding its high melting temperature. More importantly, the $sGeO_2$ film processing is very simple and environmentally friendly without any toxicity, which has potential applications in green and low-cost organic electronics in the future.

■ ASSOCIATED CONTENT

Supporting Information

The optical transmittance of interface films, AFM images of $sGeO_2$ films with varied GeO_2 solution concentrations, the decay conditions for other cell parameters including J_{sc}, V_{oc}, and FF, and optical field ($|E|^2$) distributions calculated under the consideration of the whole visible light range (300−900 nm). This material is available free of charge via the Internet at http://pubs.acs.org.

■ AUTHOR INFORMATION

Corresponding Authors

*E-mail: zkwang@suda.edu.cn.
*E-mail: lsliao@suda.edu.cn.

Notes

The authors declare no competing financial interest.

■ ACKNOWLEDGMENTS

We thank Mr. Kun Wang for his technical assistance. We acknowledge financial support from the Natural Science Foundation of China (No. 61036009, No. 61177016, and No. 21161160446), the National High-Tech Research Development Program (No. 2011AA03A110), and the Natural Science Foundation of Jiangsu Province (No. BK2010003). This is also a project funded by the Priority Academic Program Development of Jiangsu Higher Education Institutions (PAPD) and by the Fund for Excellent Creative Research Teams of Jiangsu Higher Education Institutions.

■ REFERENCES

(1) Kanno, H.; Holmes, R. J.; Sun, Y.; Cohen., S. K.; Forrest, S. R. *Adv. Mater.* **2006**, *18*, 339−342.
(2) Stubhan, T.; Li, N.; Luechinger, N. A.; Halim, S, C.; Matt, G. J.; Brabec, C. J. *Adv. Energy Mater.* **2012**, *2*, 1433−1438.
(3) Kim, D. Y.; Subbiah, J.; Sarasqueta, G.; So, F.; Ding, H.; Irfan; Gao, Y. *Appl. Phys. Lett.* **2009**, *95*, 093304.
(4) Irfan; Ding, H.; Gao, Y.; Kim, D. Y.; Subbiah, J.; So, F. *Appl. Phys. Lett.* **2010**, *96*, 073304.
(5) Li, G.; Chu, C. W.; Shrotriya, V.; Huang, J.; Yang, Y. *Appl. Phys. Lett.* **2006**, *88*, 253503.
(6) Tao, C.; Ruan, S.; Xie, G.; Kong, X.; Shen, L.; Meng, F.; Liu, C.; Zhang, X.; Dong, W.; Chen, W. *Appl. Phys. Lett.* **2009**, *94*, 043311.
(7) Frey, G. L.; Reynolds, K. J.; Barker, J. A.; Greenham, N. C.; Friend, R. H. *J. Appl. Phys.* **2002**, *92*, 7556−7563.
(8) Xu, M. F.; Cui, L. S.; Zhu, X. Z.; Gao, C. H.; Shi, X. B.; Jin, Z. M.; Wang, Z. K.; Liao, L. S. *Org. Electron.* **2013**, *14*, 657−664.
(9) You, H.; Dai, Y, F.; Zhang, Z, Q.; Ma, D, G. *J. Appl. Phys.* **2007**, *101*, 026105.
(10) Meyer, J.; Hamwi, S.; Bülow, T.; Johannes, H. H.; Riedl, T.; Kowalsky, W. *Appl. Phys. Lett.* **2007**, *91*, 113506.
(11) Janssen, A. G. F.; Riedl, T.; Hamwi, S.; Johannes, H. H.; Kowalsky, W. *Appl. Phys. Lett.* **2007**, *91*, 073519.
(12) Tokito, S.; Noda, K.; Taga, Y. *J. Phys. D: Appl. Phys.* **1996**, *29*, 2750.
(13) Jørgensen, M.; Norrman, K.; Krebs, F. C. *Sol. Energy Mater. Sol. Cells* **2008**, *92*, 686−714.
(14) Jong, M. P. D.; Ijzendoorn, L. J. V.; Voigt, M. J. A. D. *Appl. Phys. Lett.* **2000**, *77*, 2255.
(15) Wong, K. W.; Yip, H. L.; Luo, Y.; Wong, K. Y.; Lau, W. M.; Low, K. H.; Chow, H. F.; Gao, Z. Q.; Yeung, W. L.; Chang, C. C. *Appl. Phys. Lett.* **2002**, *80*, 2788.
(16) Shrotriya, V.; Li, G.; Yao, Y.; Chu, C. W.; Yang, Y. *Appl. Phys. Lett.* **2006**, *88*, 073508.
(17) Dillon, J. A.; Farnsworth, H. E. *J. Appl. Phys.* **1957**, *28*, 174−184.
(18) Fadida, S.; Eizenberg, M.; Nyns, L.; Elshocht, S. V.; Caymax, M. *Microelectron. Eng.* **2011**, *88*, 1557−1559.
(19) Hung, L. S.; Tang, C. W.; Mason, M. G. *Appl. Phys. Lett.* **1997**, *70*, 152−154.
(20) Schubert, S.; Hermenau, M.; Meiss, J.; Meskkamp, L. M.; Leo, K. *Adv. Funct. Mater.* **2012**, *22*, 4993−4999.
(21) Murase, S.; Yang, Y. *Adv. Mater.* **2012**, *24*, 2459−2462.
(22) Dong, X.; Liu, J.; Yan, J.; Wang, J.; Hong, G. *Rare Met. Mater. Eng.* **2005**, *34*, 421−424.
(23) Jasieniak, J. J.; Seifter, J.; Jo, J.; Mates, T.; Heeger, A. J. *Adv. Funct. Mater.* **2012**, *22*, 2594−2605.
(24) Yang, T.; Wang, M.; Cao, Y.; Huang, F.; Huang, L.; Peng, J.; Gong, X.; Cheng, S. Z. D.; Cao, Y. *Adv. Energy Mater.* **2012**, *2*, 523−527.
(25) Lee, Y. J.; Yi, J.; Gao, G. F.; Koerner, H.; Park, K.; Wang, J.; Luo, K.; Vaia, R. A.; Hsu, J. W. P. *Adv. Energy Mater.* **2012**, *2*, 1193−1197.
(26) Hecht, D. S.; Ramirez, R. J. A.; Briman, M.; Artukovic, E.; Chichak, K. S.; Stoddart, J. F.; Grüner, G. *Nano Lett.* **2006**, *6*, 2031−2036.
(27) Murase, S.; Yang, Y. *Adv. Mater.* **2012**, *24*, 2459−2462.
(28) Peulon, S.; Lincot, D. *Adv. Mater.* **1996**, *8*, 166−170.
(29) Chen, Z.; Zhang, H.; Xing, Z.; Hou, J.; Li, J.; Wei, H.; Tian, W.; Yang, B. *Sol. Energy Mater. Sol. Cells* **2013**, *109*, 254−261.
(30) Minami, T.; Nishi, Y.; Miyata, T. *Appl. Phys. Express* **2013**, *6*, 044101.
(31) Choi, M. K.; Kim, J.-H.; Yoon, H.; Tahk, D.; Seo, S.; Shin, K.; Lee, H. H. *J. Nanosci. Nanotechnol.* **2012**, *12*, 623−628.
(32) Dean, J. A. *Lange's Chemistry Handbook*; McGraw-Hill Companies, Inc.: New York, 1999; Version 15th.
(33) Pokrovvski, G. S.; Schott, J. *Geochim. Cosmochim. Acta* **1998**, *62*, 1631−1642.
(34) Perego, M.; Scarel, G.; Fanciulli, M.; Fedushkin, I. L.; Skatova, A. A. *Appl. Phys. Lett.* **2007**, *90*, 053508.
(35) Bringans, R. D.; Uhrberg, R. I. G.; Bachrach, R. Z. *Phys. Rev. B* **1987**, *36*, 9569−9580.
(36) Lange, T.; Njoroge, W.; Weis, H.; Beckers, M.; Wuttig, M. *Thin Solid Films* **2000**, *365*, 82−89.
(37) Pettersson, L. A. A.; Roman, L. S.; Inganäs, O. *J. Appl. Phys.* **1999**, *86*, 487−496.
(38) Stübinger, T.; Brütting, W. *J. Appl. Phys.* **2001**, *90*, 3632−3641.
(39) Hänsel, H.; Zettl, H.; Krausch, G.; Kisselev, R.; Thelakkat, M.; Schmidt, H. W. *Adv. Mater.* **2003**, *15*, 2056−2060.
(40) Kim, J. Y.; Kim, S. H.; Lee, H. H.; Lee, K.; Ma, W. L.; Gong, X.; Heeger, A. J. *Adv. Mater.* **2006**, *18*, 572−576.
(41) Liu, J.; Shao, S. Y.; Fang, G.; Meng, B.; Xie, Z. Y.; Wang, L. X. *Adv. Mater.* **2012**, *24*, 2774−2779.

(42) Jin, H.; Tao, C.; Velusamy, M.; Aljada, M.; Zhang, Y. L.; Hambsch, M.; Burn, P. L.; Meredith, P. *Adv. Mater.* **2012**, *24*, 2572−2577.
(43) Salinas, J. F.; Yip, H. L.; Chueh, C. C.; Li, C. Z.; Maldonado, J. L.; Jen, A. K. Y. *Adv. Mater.* **2012**, *24*, 6362−6367.
(44) Walheim, S.; Schäffer, E.; Mlynek, J.; Steiner, U. *Science* **1999**, *283*, 520−522.
(45) Park, S. H.; Roy, A.; Beaupré, S.; Cho, S.; Coates, N.; Moon, J. S.; Moses, D.; Leclerc, M.; Lee, K.; Heeger, A. J. *Nat. Photonics* **2009**, *3*, 297−302.
(46) Snaith, H. J.; Greenham, N. C.; Friend, R. H. *Adv. Mater.* **2004**, *16*, 1640−1645.
(47) Melzer, C.; Koop, E. J.; Mihaletchi, V. D.; Blom, P. W. M. *Adv. Funct. Mater.* **2004**, *14*, 865−870.
(48) Steirer, K. X.; Ndione, P. F.; Widjonarko, N. E.; Lloyd, M. T.; Meyer, J.; Ratcliff, E. L.; Kahn, A.; Armstrong, N. R.; Curtis, C. J.; Ginley, D. S.; Berry, J. J.; Olson, D. C. *Adv. Energy Mater.* **2011**, *1*, 813−820.
(49) Barbu, I.; Wienk, M. M.; Janssen, R. A. J. *Appl. Phys. Lett.* **2007**, *91*, 113520.
(50) Hadipour, A.; Boer, B.; Blom, P. W. M. *J. Appl. Phys.* **2007**, *102*, 074506.
(51) Andersson, B. V.; Huang, D. M.; Moulé, A. J.; Inganäs, O. *Appl. Phys. Lett.* **2009**, *94*, 043302.
(52) Schueppel, R.; Timmreck, R.; Allinger, N.; Mueller, T.; Furno, M.; Uhrich, C.; Leo, K.; Riede, M. *J. Appl. Phys.* **2010**, *107*, 044503.
(53) Lin, H. W.; Chiu, S. W.; Lin, L. Y.; Hung, Z. Y.; Chen, Y. H.; Lin, F.; Wong, K. T. *Adv. Mater.* **2012**, *24*, 2269−2272.
(54) Huang, J.; Xu, Z.; Yang, Y. *Adv. Funct. Mater.* **2007**, *17*, 1966−1973.
(55) Guo, T. F.; He, G.; Pyo, S.; Yang, Y. *Appl. Phys. Lett.* **2002**, *80*, 4042.
(56) Woudenbergh, T. V.; Wildeman, J.; Blom, P. W. M.; Bastiaansen, J. J. A. M.; Vos, B. L. *Adv. Funct. Mater.* **2004**, *14*, 677−683.
(57) Leever, B. J.; Bailey, C. A.; Marks, T. J.; Hersam, M. C.; Durstock, M. F. *Adv. Energy Mater.* **2012**, *2*, 120−128.
(58) Belmonte, G. G.; Munar, A.; Barea, E. M.; Bisquert, J.; Ugarte, I.; Pacios, R. *Org. Electron.* **2008**, *9*, 847−851.
(59) Macdonald, J. R. *Impedance spectroscopy−Emphasizing solid materials and systems*; John Wiley & Sons: New York, 1987.
(60) Pingree, L. S. C.; Scott, B. J.; Russell, M. T.; Marks, T. J.; Hersam, M. C. *Appl. Phys. Lett.* **2005**, *86*, 073509.
(61) Pingree, L. S. C.; Russell, M. T.; Marks, T. J.; Hersam, M. C. *J. Appl. Phys.* **2006**, *100*, 044502.
(62) Radecka, M.; Wierzbicka, M.; Rekas, M. *Phys. B* **2004**, *351*, 121−128.
(63) Hsu, C. H.; Mansfeld, F. *Corrosion* **2001**, *57*, 747−748.
(64) Nicollian, E. H.; Goetzberger, A. *Bell Syst. Tech. J.* **1967**, *46*, 1055−1133.
(65) Okachi, T.; Nagase, T.; Kobayashi, T.; Naito, H. *Jpn. J. Appl. Phys.* **2008**, *47*, 8965−8972.
(66) Nagase, T.; Kobayashi, T.; Naito, H. *Appl. Phys. Lett.* **2009**, *94*, 043301.
(67) Chen, C. C.; Huang, B. C.; Lin, M. S.; Lu, Y. J.; Cho, T. Y.; Chang, C. H.; Tien, K. C.; Liu, S. H.; Ke, T. H.; Wu, C. C. *Org. Electron.* **2010**, *11*, 1901−1908.
(68) Zhang, L.; Taguchi, D.; Li, J.; Manaka, T.; Iwamoto, M. *Appl. Phys. Lett.* **2011**, *98*, 092109.
(69) Cai, S. D.; Gao, C. H.; Zhou, D. Y.; Gu, W.; Liao, L. S. *ACS Appl. Mater. Interfaces* **2011**, *4*, 312−314.
(70) Sze, S. M. *Physics of Semiconductor Device*, 2nd ed.; Wiley: New York, 1981.
(71) Scott, J. C. *J. Vac. Sci. Technol., A* **2003**, *21*, 521−531.
(72) Wang, Z. K.; Lou, Y. H.; Naka, S.; Okada, H. *Appl. Phys. Lett.* **2011**, *98*, 063302.